2025 IEEE 11th International Conference on Control Science and Systems Engineering (ICCSSE) | 979-8-3315-7669-1/25/$31.00 ©2025 IEEE | DOI: 10.1109/ICCSSE67426.2025.11552484

Optimal Trajectory Generation and Feedback Tension Control of a Robotic Space Tether Launching System

Shuai Liu
Mechanical and Aerospace Engineering
The Hong Kong University of Science and Technology
Hong Kong, China
sliucr@connect.ust.hk

Sichen Wang
Mechanical and Aerospace Engineering
The Hong Kong University of Science and Technology
Hong Kong, China
swangfz@connect.ust.hk

Molong Duan*
Mechanical and Aerospace Engineering
The Hong Kong University of Science and Technology
Hong Kong, China
duan@ust.hk
*Corresponding author

***Abstract*—In space, accurately delivering payloads enables inspection, monitoring, and debris-removal missions. Space tether systems have long been explored for momentum exchange, deorbiting, and inspection. However, existing methods have not considered using a robotic arm in a space tether system to actively accelerate and launch payloads. Also, most prior models neglect the tether mass or approximate it as massless. To close these gaps, a robotic space tether launching system with a unified modeling–control framework is established. A full nonlinear model is derived considering the tether's mass distributions and directional tension coupling. An optimal control scheme is formulated that combines feedforward profiles with tension-feedback regulation for robustness to uncertainties and disturbances. Simulation results verify accurate targeting with specified terminal velocity, enabling propellant-free, high-precision deployment.**

***Keywords*—Space tether, robotic launching, dynamic modeling, optimal control**

I. Introduction

Space tether is a concept with many applications, including satellite servicing [1] and cargo transfer between spacecraft, and also shows promise for precision payload delivery in space operations removing space debris[2]. Similar tether systems have already been applied on GEO satellites for deploying space robots[3], space tether-net system capture and delivery[4]. Due to structural and actuation constraints, traditional rigid manipulators are inherently limited in end-effector speed and workspace; by contrast, tether-assisted systems exploit centrifugal force for velocity amplification and offer a promising alternative, but their dynamics are strongly influenced by tether mass and directional tension coupling[5] and the nonlinear characteristics exhibited by the cable system[6], posing significant challenges for modeling and control[7].

Existing research on space tethered systems spans multiple domains. Early foundational work by Cartmell & McKenzie [8] comprehensively reviewed space tether applications and dynamics, highlighting the complex nonlinearities inherent in these systems. For robotic throwing mechanisms, Williams [9] explored optimal deployment strategies for tethered satellite formation spinning in the orbital plane, while Jin & Hu [10] investigated optimal control of tethered subsatellites with three degrees of freedom. In tension control, Chu [11] developed a hybrid tension control method to stabilize a satellite system tethered to large space debris. More recently, Lu et al. [12] addressed saturated control for space tether systems maneuvering between arbitrary spinning orientations, tackling input saturation challenges during large-scale maneuvers. For trajectory optimization, Zhang et al. [13] developed a computational feedback control framework for flexible tethered space systems, Hong et al. [14] reviewed the performance of various deployment controllers for Tethered Space Systems (TSS), while Longuski et al. [15] provided comprehensive coverage of optimal control applications in aerospace systems.

Despite substantial progress, critical gaps remain. Owing to complexity, most studies either neglect tether mass or treat the tether as massless, thereby simplifying tension dynamics; consequently, the coupled dynamics between variable-length tethers and rotating systems are often over-simplified, particularly during the transition from rotational acceleration to the controlled-release phase. However, as space tethers are increasingly applied for payload delivery, the dynamic effects induced by tether mass have become too significant to ignore. Moreover, existing control approaches typically treat the acceleration and controlled-release phases in isolation, lacking a unified framework for integrated control across both phases, which constrains the optimization of control performance. To address these shortcomings, this work proposes a model that systematically accounts for tether mass effects, directional tension coupling, and seamless phase transitions.

Building on this, an innovative tether-assisted deployment concept was considered that employs a robotic arm with an integrated winch to control the release and tensioning of the payload-connected tether, establishing a dedicated nonlinear dynamic model of the robotic space tether launching system, which enables a unified control framework that spans the entire deployment process. a combined feedforward (FF) and a model predictive control (MPC)-based tension-feedback law was designed to generate optimal control inputs through receding horizon optimization, ensuring robust targeting under uncertainties and disturbances while adhering to tether tautness and actuator constraints. This capability enables precise payload deployment for on-orbit applications such as celestial body inspection, satellite monitoring, and active space debris removal. In summary, this paper makes three primary contributions:

- An innovative concept of space tether launching and control system exploiting robotic manipulators is proposed, constituting rotational acceleration and controlled release phases;

- A dedicated nonlinear dynamic model of the robotic space tether launching system is developed, considering the tether's mass distributions and directional tension throughout the two phases;
- A control framework integrating feedforward and NMPC-driven feedback was developed to proactively compensate for uncertainties and disturbances.

The remainder of this paper is organized as follows. Section II presents the dynamic modeling of the robotic space tether launching system. Section III introduces the optimal and NMPC control strategy. Section IV provides simulation results followed by the conclusion in Section V.

II. Dynamic Modeling of the Tether Launching System

In space operations, the absence of gravitational and atmospheric forces enables the use of novel propulsion-free launching methods. This work investigates a strategy where a payload, tethered to a robotic arm via a winch system, is accelerated and launched toward a target point. As Fig. 1 shows, the system comprises two main operational phases:

- Phase A - rotational acceleration: The robotic arm rotates at a constant angular velocity, while accelerating the payload by slowly paying out the tether. The payload is released at a precisely calculated instant.
- Phase B – controlled release: After release, the payload enters a free-flight phase. It remains connected to the winch via the tether. A control torque applied to the winch modulates the tether tension, enabling trajectory corrections to ensure the payload arrives at the target.

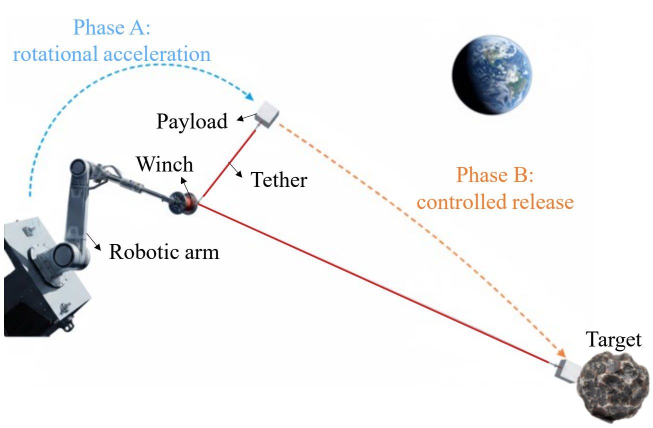

Fig. 1. Schematic illustration of the two operational phases in the robotic space tether launching system

A. Rotational Acceleration

As the controlled release phase of Fig. 2 shows, the objective of this phase is to accelerate the payload of mass m from rest to a designated launch velocity v_0, which typically exceeds the maximum permissible linear speed v_m of the robotic arm's tip. The acceleration is achieved by spinning the arm at a constant rate while slowly paying out the tether. Let $r(t)$ denote the length of tether paid out from the winch exit point A located at the arm's tip. Given that the angular velocity of the rotation is ω_0, to achieve the target launch velocity v_0 at the release time t_{rel}, the required tether length deployed at t_{rel} is found by

$$r_0 = \frac{v_0}{\omega_0} - R_a, \tag{1}$$

where R_a is the radius of the rotation in the robotic arm. The dynamics of the tether itself, which is modeled as inextensible and has a linear mass density ρ_c, is considered to determine the tension profile.

A coordinate p along the tether is defined, where $p=0$ corresponds to the arm's tip (winch exit point) and $p=r(t)$ corresponds to the payload end. For a tether segment at position p, its radial acceleration relative to O is composed of the translational acceleration of the $r(t)$ and the centripetal acceleration, expressed as:

$$a_r(p,t) = \ddot{r}(t) - \omega_0^2(R_a + p) \tag{2}$$

The tension force $T(p,t)$ within the tether balances the inertial forces of the tether segments beyond it. This leads to a differential equation describing the tension gradient along the tether:

$$\frac{\partial T(p,t)}{\partial p} = \rho_c[\omega_0^2(R_a+p) - \ddot{r}(t)]. \tag{3}$$

This equation is integrated from the payload inward to find the tension at any point. The boundary condition is defined at the payload $p=r(t)$, where the tension must provide the necessary centripetal force for its circular motion:

$$T(r(t),t) = m[\omega_0^2(R_a + r(t)) - \ddot{r}(t)]. \tag{4}$$

Integrating the tension gradient from $p=r(t)$ to $p=0$ and applying this boundary condition yields the tension at the winch exit point A:

$$T_w(t) = \left[m(R_a+r) + \rho_c\left(R_a r + \frac{1}{2}r^2\right)\right]\omega_0^2 - (m+\rho_c r)\ddot{r}. \tag{5}$$

The motion of the winch, which controls the deployment rate $\dot{r}(t)$, is governed by its own dynamics. The kinematic relationship between the paid-out tether length $r(t)$ and the angular displacement of the winch $\theta_s(t)$ (with radius r_s) is:

$$\dot{r}(t) = -r_s\,\omega_s(t), \tag{6}$$

where $\omega_s(t)$ is the winch's angular velocity, defined such that a positive value corresponds to reeling in. The winch dynamics, which has an effective moment of inertia J_s and a viscous damping coefficient b, is derived from the balance of torques:

$$J_s\,\dot{\omega}_s(t) = \tau(t) - r_s\,T_w(t) - b\,\omega_s(t),$$
$$J_s = J_{s0} - \rho_c r_s{}^2 r, \tag{7}$$

where, J_{s0} is the moment of inertia of the winch when all the tether is wound on the winch, $\tau(t)$ is the control torque input, which typically has a negative value, meaning to prevent the movement of the tether, $r_s T_w(t)$ is the load torque from the tether tension, and $b\omega_s(t)$ is the resisting torque due to damping.

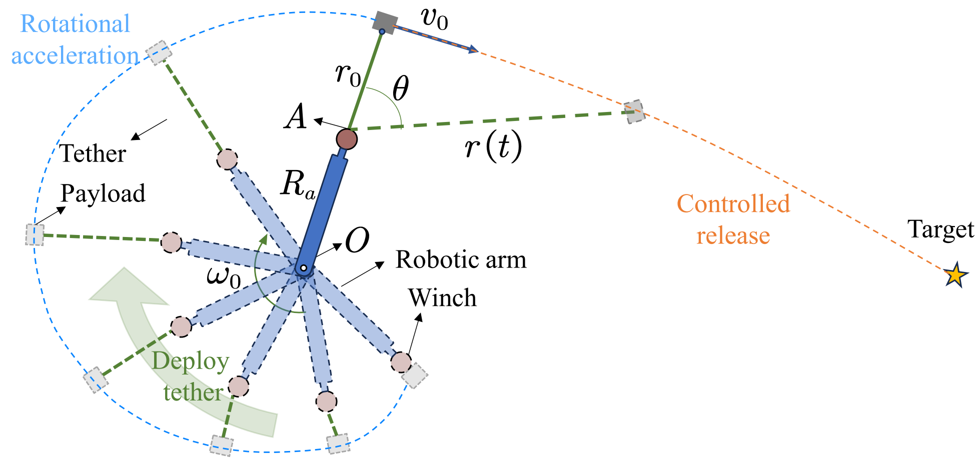

Fig. 2. The illustration of rotational acceleration (Phase A) and controlled release (Phase B).

B. Controlled Release

Following the release of the payload at time t_{rel}, the system enters a controlled release phase. The winch exit is now fixed in the inertial frame, and the payload's motion is influenced solely by the tension in the tether, which is controlled by the torque applied to the winch. The system is subject to no external torque about the fixed pivot point, leading to the motion in a two-dimensional plane and the conservation of angular momentum. The process is illustrated in the controlled release phase of Fig. 2. The polar angle of the payload is denoted by $\theta(t)$ and its angular velocity by $\dot{\theta}(t)$. The effective moment of inertia of the system (payload and tether) about the pivot is given by:

$$I(r) = m\,r^2 + \frac{1}{3}\rho_c\,r^3. \tag{8}$$

The constant angular momentum h is therefore:

$$h = I(r)\,\dot{\theta}. \tag{9}$$

This relationship determines the evolution of the angular velocity as the tether length $r(t)$ changes:

$$\dot{\theta}(t) = \frac{h}{I(r(t))}. \tag{10}$$

The tangential velocity component of the payload is consequently:

$$v_\theta(t) = r(t)\,\dot{\theta}(t) = \frac{h\,r(t)}{I(r(t))}. \tag{11}$$

The radial acceleration of a point on the tether located at p is derived as:

$$a_r(p,t) = \ddot{r}(t) - p\,\dot{\theta}(t)^2. \tag{12}$$

Integrating the force balance along the tether, considering the boundary condition at the payload end $p = r$, yields the tension distribution:

$$T(p,t) = m\left[r\dot{\theta}^2 - \ddot{r}\right] + \rho_c\left[\frac{1}{2}(r^2 - p^2)\dot{\theta}^2 - (r-p)\ddot{r}\right] \tag{13}$$

The tension at $p = r(t)$ is:

$$T_{\text{end}} = m\left(r\,\dot{\theta}^2 - \ddot{r}\right). \tag{14}$$

The tension at $p = 0$ is a critical value for winch dynamics:

$$T_0 = \left[m\,r + \frac{1}{2}\rho_c\,r^2\right]\dot{\theta}^2 - (m + \rho_c\,r)\ddot{r} \tag{15}$$

Substituting (15) and (6) into the winch dynamics equation (7) yields the explicit form for the radial acceleration:

$$\ddot{r} = \frac{C(r) - \frac{\tau + b\,\dot{r}/r_s}{r_s}}{M_{\text{eff}}}, \qquad \dot{\theta} = \frac{h}{I(r)}, \tag{16}$$

where the effective mass term and the centrifugal force term are:

$$M_{\text{eff}} = m + \frac{J_{s0}}{r_s^2}, \qquad C(r) = [mr + \frac{1}{2}\rho_c r^2]\dot{\theta}^2. \tag{17}$$

C. Reachable Workspace Analysis

The maximum release speed of the Phase A is constrained by the maximum angular velocity of the robotic arm $\omega_{\max}$ and the maximum centrifugal tension $F_{c,\max}$ the arm can withstand. The tension at the winch end is given by:

$$T_{0,w} = \left[m(R_a + r) + \rho_c\left(R_a r + \frac{1}{2}r^2\right)\right]\omega_0^2. \tag{18}$$

When the condition $\omega_0 = \omega_{\max}$ is satisfied to fully exploit the robotic arm's performance, the constraint $T_{0,w} \le F_{c,\max}$ yields a quadratic inequality in r:

$$\left[m(R_a + r) + \rho_c\left(R_a r + \frac{1}{2}r^2\right)\right]\omega_{\max}^2 - F_{c,\max} \le 0. \quad (19)$$

Taking the positive root of the corresponding equation and further constraining it by the maximum tether length, the effective maximum achievable radius is:

$$r_{max} = \frac{-m + \sqrt{m^2 + \rho_c^2 R_a^2 + \dfrac{2F_{c,\max}}{\rho_c\,\omega_{\max}^2}}}{\rho_c}. \quad (20)$$

In the phase of controlled release, the maximum range attainable appears when $\tau = u_{min}$, where u_{min} is the minimal torque to keep the cable taut, providing a margin for control. The maximum deployable radius is computed by integrating the coupled dynamics (16) until the first turning point t^* of the radial motion is detected, defined as the earliest time when

$$\dot{r}(t^*) = 0,\ \ddot{r}(t^*) \le 0. \quad (21)$$

The corresponding radius $r(t^*)$ is accepted as the attainable range, further bounded by the maximum tether length r_{cable}:

$$r_{\max}^f = \min\{r(t^*),\ \ r_{\text{cable}}\}. \quad (22)$$

This result $r_{\max}^f$ provides a fundamental performance limit for the system's reachable workspace under passive deployment.

III. Optimal and Feedback Control Strategy

A minimal state-space model for the flight phase can be defined using three states. The state vector and control input are:

$$\mathbf{x} = [r,\ \dot{r},\ \theta]^\top,\ u = \tau. \quad (23)$$

The corresponding nonlinear state equations are:

$$\dot{r} = \dot{r},\quad \ddot{r} = \frac{C(r) - \frac{u + b\,\dot{r}/r_s}{r_s}}{M_{\text{eff}}},\quad \dot{\theta} = \frac{h}{I(r)}. \quad (24)$$

A. Optimal Trajectory Generation

An optimal control problem (OCP) is constructed to generate the optimal FF trajectory of the tether length and the winch's torque. The solution must adhere to several path constraints. For the model to remain valid, the tether must remain under tension. This imposes constraints on the radial acceleration, derived from requiring non-negative tension at both ends of the tether:

$$\begin{aligned} &T_{\text{end}} \ge 0 \ \Rightarrow\ \ddot{r} \le r\dot{\theta}^2, \\ &T_0 \ge 0 \ \Rightarrow\ \ddot{r} \le \frac{C(r)}{m + \rho_c r}. \end{aligned} \quad (25)$$

Furthermore, the winch actuator is subject to physical limits on its torque:

$$u_{\min} < u < u_{\max}, \quad (26)$$

where $u_{\max}$ is the maximum torque the winch can provide. The initial conditions are defined by the state at the release time: r_0, θ_0 and ω_0. Let r_f be the tether length when the payload reaches the target point. The terminal conditions at the final time t_f are defined by the target point and the desired terminal speed v_s:

$$\begin{aligned} &r(t_f) = r_f,\ \theta(t_f) = \theta_f, \\ &v_{s_{\min}}^2 \le \dot{r}(t_f)^2 + \left(r_f\dot{\theta}(t_f)\right)^2 \le v_{s_{\max}}^2, \\ &\theta_{v_{\min}} \le \arctan 2\left(r_f\dot{\theta}(t_f), \dot{r}(t_f)\right) \le \theta_{v_{\max}}. \end{aligned} \quad (27)$$

where r_f and θ_f are the polar coordinates of the target point, $v_{s_{\min}}$ and $v_{s_{\max}}$ define the minimum and maximum allowable speeds, and the velocity direction $\arctan 2\left(r_f\dot{\theta}(t_f), \dot{r}(t_f)\right)$ is constrained to lie within a specified range defined by $\theta_{v_{\min}}$ and $\theta_{v_{\max}}$. The OCP minimizes a cost functional J that penalizes control effort, tension, and radial velocity to achieve a smooth and efficient trajectory expressed as:

$$J = \int_0^{t_f} \left(w_\tau\, u(t)^2 + w_T\, T_0(t)^2 + w_{\dot{r}}\, \dot{r}(t)^2\right) dt \quad (28)$$

where w_τ, w_T, and $w_{\dot{r}}$ are non-negative weighting coefficients that adjust the priority of minimizing control torque, tether tension at the winch, and radial jerk, respectively. The final time t_f may be fixed or free, depending on the problem formulation. Solve this constrained OCP and obtain the reference trajectory $\mathbf{x}_{ref}$ and the winch's torque input u_{ref}, as well as the initial condition $\mathbf{x}_0$.

B. NMPC-driven Feedback Control

The whole control block diagram is as Fig. 3. The continuous-time dynamics (24) are discretized using the forward Euler method, yielding the discrete-time system:

$$\mathbf{x}_{k+1} = \mathbf{f}_d(\mathbf{x}_k, u_k). \quad (29)$$

The controller's objective is to track an offline-computed optimal reference trajectory $\mathbf{x}_{ref}$ by minimizing the tracking error defined as

$$\mathbf{e}_k = \mathbf{x}_k - \mathbf{x}_k^{\text{ref}}. \quad (30)$$

The control deviation is defined as

$$\delta u_k = u_k - u_k^{\text{ref}}. \quad (31)$$

An NMPC is employed to attenuate the deviation while explicitly enforcing input and state constraints. At each time step k, a finite-horizon optimal control problem is solved online over a prediction horizon of N steps. The cost function is a quadratic form in the error state and control deviation, given by

$$\begin{aligned} &\min_{\delta u_{k|k},\dots,\delta u_{k+N-1|k}} \sum_{i=0}^{N-1} \left(\mathbf{e}_{k+i|k}^\top \mathbf{Q}\,\mathbf{e}_{k+i|k} + \delta u_{k+i|k}^\top R\,\delta u_{k+i|k}\right) + \mathbf{e}_{k+N|k}^\top \mathbf{P}\,\mathbf{e}_{k+N|k}, \\ &\text{s.t.}\quad \mathbf{e}_{k|k} = \mathbf{x}_k - \mathbf{x}_k^{\text{ref}} \\ &\qquad\ \ \mathbf{e}_{k+i+1|k} = \mathbf{f}_d\left(\mathbf{x}_{k+i|k}, u_{k+i|k}\right) - \mathbf{x}_{k+i+1}^{\text{ref,b}}. \end{aligned} \quad (32)$$

where $\mathbf{Q}$, R, $\mathbf{P}$ are the tuning matrices. In order to avoid a reduction of the prediction length when the horizon extends beyond the last sampling time t_f, the reference sequence that enters the optimisation is extended by holding its terminal value constant, which can be expressed as:

$$\mathbf{x}_{k+i}^{\mathrm{ref,b}} = \begin{cases} \mathbf{x}_{k+i}^{\mathrm{ref}} & \text{if } t_k + i \cdot \Delta t < t_f \\ \mathbf{x}_{\mathrm{final}}^{\mathrm{ref}} & \text{if } t_k + i \cdot \Delta t \geq t_f \end{cases}. \tag{33}$$

After the optimisation is solved only the first input correction $\delta u_{k|k}$ is applied. The horizon is then shifted forward, the problem is reformulated with the new measurements, and the procedure is repeated.

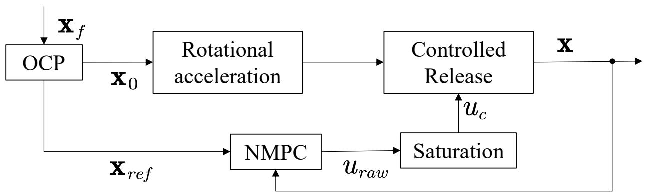

Fig. 3. The control block diagram of the two-loop control architecture

IV. Simulation Results

A. Simulation Setup

To verify the effectiveness of the proposed tether-assisted deployment system, a simulation was conducted in a zero-gravity vacuum environment. Fig. 4 schematizes the model setup. The model consists of a UR5e robotic arm—whose first joint allows continuous rotation—fitted with a simulated winch on its end-effector. A 1 kg payload is connected to the winch via the tether.

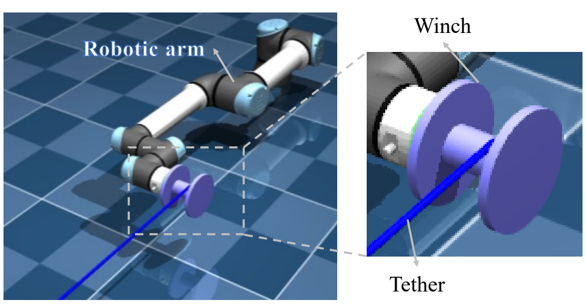

Fig. 4. Simulation model of the robotic space tether launching system

The manipulation process comprises two stages: In Phase A, the arm spins at a constant velocity while deploying the tether to accelerate the payload, which is released at a calculated instant. In Phase B, the payload enters free-flight, and a control torque applied to the winch modulates tether tension to perform real-time trajectory corrections for accurate targeting.

B. Simulation Results

In the first stage, an optimal control problem was solved to obtain a reference trajectory for the FF control. Specifically, the target location is set as $r_f = 10$ m, $\theta_f = 1.2$ rad . The solution gives the initial condition as:

$$r_0 = 3.0 \text{ m}, \ \theta_0 = 2.9 \text{ rad}, \ \omega_0 = -1.1 \text{ rad/s}. \tag{34}$$

Also, the optimal trajectory of input torque and the corresponding $r(t)$ are summarized as Fig. 5. The reference trajectory in Fig. 5 (a) shows a trend of expanding outward in a spiral shape, which is due to the non-zero torque acting on the winch system.

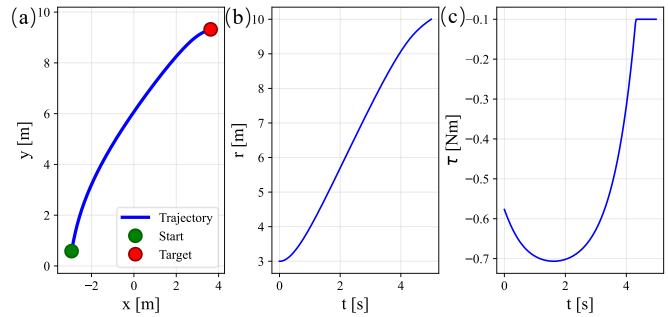

Fig. 5. The optimal FF trajectory of the controlled release phase

To emulate the model error, the initial velocity v_0 and angle θ_0 are perturbed. Simulations were conducted under both FF and NMPC on this basis, and the results are as Fig. 6, where (a) presents the reference trajectory and trajectories obtained under FF and NMPC, (b), (c), and (d) show the tracking error of the trajectory, the radius r , and the angle θ .

The Cartesian trajectory and the tracking error in Fig. 6 (a) and (b) show that the FF trajectory exhibits a significant and growing deviation, culminating in a final position error of 0.40 m. In contrast, the NMPC trajectory closely adheres to the reference, achieving a maximum tracking error of only 0.02 m, realizing a deduction of 95%. In the radius tracking error shown in Fig. 6 (c), the NMPC scheme initially exhibits a transient growth in the opposite direction before converging toward zero. This occurs because the NMPC action prioritizes rapid correction of the angular deviation, temporarily trading off radial accuracy. In contrast, the radius tracking error of FF remains persistently large. The final radius tracking error is 159.8 mm for FF and 3.5 mm for NMPC, corresponding to a 97.8% reduction. Between 4.2 and 5 seconds, an increase in the radius tracking error is observed, which is attributed to the control input reaching actuator saturation. In the angle tracking error shown in Fig. 6 (d), the FF strategy reaches a final 2.1°, while the NMPC controller effectively suppresses the error within ±0.1° throughout the trajectory, which further demonstrates the robustness and effectiveness of the NMPC control strategy in the robotic space tether launching system.

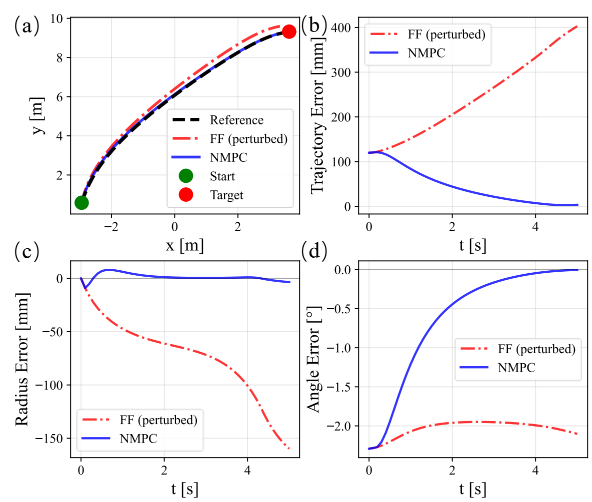

Fig. 6. The NMPC result compared with the FF reference under perturbation

V. CONCLUSION

This study has introduced a dynamic modeling and control framework for a robotic space tether launching system, aiming to achieve precise payload delivery with constrained mechanical actuation. The proposed approach integrates a two-phase control strategy: rotational acceleration through progressive tether deployment, followed by the controlled release via torque regulation at the winch. The model fully captures nonlinear tether dynamics, including mass, tension, and directional misalignment effects. An optimal control-based feedforward trajectory, enhanced by an NMPC strategy using tether length and angle feedback, significantly improves targeting accuracy under disturbances. Simulations confirm that the payload reaches the desired position with specified terminal velocity, and comparative tests demonstrate the method's strong capability in compensating for initial perturbations. The results highlight the feasibility and effectiveness of using tether-based passive actuation mechanisms to achieve high-precision control in space applications. The approach offers a novel solution for extending the capabilities of robotic systems where direct propulsion or high-speed actuation is constrained, opening new possibilities in autonomous payload delivery, satellite servicing, and orbital maneuvering under limited-resource conditions.

Subsequent research will focus on robust control synthesis using disturbance observers and adaptive laws for uncertain environments and experimental validation through ground-based microgravity emulators. These efforts aim to enhance system reliability for orbital deployment missions.

ACKNOWLEDGMENT

This work was supported by the Frontier Technology Research for Joint Institutes with industry scheme under grant OKT24EG07, the Research Grants Council (RGC) of the Government of Hong Kong Special Administrative Region (HKSAR) with RGC/ECS Project No. 26215824, and the Innovation and Technology Commission (ITC) of the HKSAR with the ITF Project No. GHP/170/22SZ.

REFERENCES

[1] L. Li, A. Li, H. Lu, and C. Wang, "Along-track deployment control of space tether system for SAR-GMTI mission," Acta Astronaut., vol. 226, pt. 1, pp. 102‑111, 2025, doi: 10.1016/j.actaastro.2024.10.041.

[2] H. Yang, C. Wang, H. Lu, and A. Li, "Analysis of fly-around mission with spinning tether system for space station observation," Acta Astronaut., vol. 226, pt. 1, pp. 137 ‑ 146, 2025, doi: 10.1016/j.actaastro.2024.10.032.

[3] P. Huang *et al.*, "A review of space tether in new applications," *Nonlinear Dyn.*, vol. 94, no. 1, pp. 1–19, 2018, doi: 10.1007/s11071-018-4389-5.

[4] M. Li, S. Yue, W. Shi, Z. Zhao, and Z. Du, "Experiments and dynamic analysis on the closure of tether-net capture for space debris," Acta Astronaut., vol. 234, pp. 619 ‑ 631, 2025, doi: 10.1016/j.actaastro.2025.05.035.

[5] W. Zhu, Z. Pang, J. He, and Z. H. Zhu, "Dynamic modeling and prediction of post launch rebound mechanism of tethered space net," Appl. Math. Model., vol. 140, Art. no. 115861, 2025, doi: 10.1016/j.apm.2024.115861.

[6] W. Zhu, Z. Pang, J. He, J. Guo, W. Zhao, Z. Du, and Z. H. Zhu, "Tensile experiment based nonlinear tether element model for tethered space net," Acta Astronaut., vol. 228, pp. 643 ‑ 651, 2025, doi: 10.1016/j.actaastro.2024.12.041.

[7] P. Huang, F. Zhang, J. Cai, D. Wang, Z. Meng, and J. Guo, "Dexterous Tethered Space Robot: Design, Measurement, Control, and Experiment," *IEEE Trans. Aerosp. Electron. Syst.*, vol. 53, no. 3, pp. 1452–1468, 2017, doi: 10.1109/TAES.2017.2671558.

[8] M. P. Cartmell and D. J. McKenzie, "A review of space tether research," *Prog. Aerosp. Sci.*, vol. 44, no. 1, pp. 1–21, 2008, doi: 10.1016/j.paerosci.2007.08.002.

[9] P. Williams and P. Trivailo, "On the optimal deployment and retrieval of tethered satellites," *41st AIAA/ASME/SAE/ASEE Jt. Propuls. Conf. Exhib.*, no. July, 2005, doi: 10.2514/6.2005-4291.

[10] D. P. Jin and H. Y. Hu, "Optimal control of a tethered subsatellite of three degrees of freedom," *Nonlinear Dyn.*, vol. 46, no. 1–2, pp. 161–178, 2006, doi: 10.1007/s11071-006-9021-4.

[11] Z. Chu, J. Di, and J. Cui, "Hybrid tension control method for tethered satellite systems during large tumbling space debris removal," *Acta Astronaut.*, vol. 152, no. August, pp. 611–623, 2018, doi: 10.1016/j.actaastro.2018.09.016.

[12] H. Lu, C. Wang, C. Sun, A. Li, and Y. M. Zabolotnov, "Saturated Control of Space Tether System for Maneuvering Between Arbitrary Spinning Orientations," *J. Guid. Control. Dyn.*, vol. 47, no. 10, pp. 2173–2181, Oct. 2024, doi: 10.2514/1.G008252.

[13] Q. Zhang and Z. H. Zhu, "Computational control framework for tethered space systems using finite element method," Acta Astronaut., vol. 228, pp. 595‑606, 2025, doi: 10.1016/j.actaastro.2024.12.013.

[14] A. A. T. Hong, R. Varatharajoo, and Y.-C. Chak, "Review of deployment controllers for space tethered system," Adv. Space Res., vol. 75, no. 4, pp. 3933‑3949, 2025, doi: 10.1016/j.asr.2024.11.061.

[15] J. M. Longuski, J. J. Guzmán, and J. E. Prussing, *Optimal Control with Aerospace Applications*. New York, NY: Springer New York, 2014.